Use of Enhanced-Resolution QuikSCAT/SeaWinds Data for Operational Ice Services and Climate Research: Sea Ice Edge, Type, Concentration, and Drift

Jörg Haarpaintner and Gunnar Spreen

***Abstract*—Enhanced-resolution QuikSCAT/SeaWinds (QS_{er}) data recently entered the daily ice chart operation of the national ice services. Algorithms have been developed to extract four important sea ice parameters from this data over the whole Arctic: sea ice edge, type, concentration, and drift. This paper will summarize the different algorithms with a more detailed presentation of the sea ice concentration (IC) algorithm that has not been previously published. The sea ice edge can be detected to IC as low as 10%. Sea ice types can be roughly separated by a single threshold of −12 dB in the horizontal polarization. The IC algorithm gives reasonable qualitative results, separating into three classes: high, medium, and low ICs. It resolves even some characteristic ice features in the marginal ice zone and dynamic areas like the Fram Strait. However, it is very empirical and quantitatively not reliable. Sea ice drift can be determined with an accuracy of about 2.6 cm/s for a 48-h drift. Operating since 1999, QS is an important global data set for climate research, and two crucial applications how these sea ice products can be used for climate research are presented: the seasonal evolution of the sea ice cover and the export of sea ice volume through Fram Strait.**

***Index Terms*—Arctic, remote sensing, scatterometry, sea ice.**

I. Introduction

SEA ICE plays a key role in the Earth's climate and its observation by satellite remote sensing techniques is an important task in climate research. Additionally, sea ice presents a major risk for marine activities and the national ice services are required to produce reliable ice charts to secure navigation and other offshore activities. In particular microwave sensors are crucial tools because of their independence of sunlight and cloud-penetrating capability. The SeaWinds instrument on QuikSCAT (QS), launched in June 1999, is an active Ku-band dual-polarized scanning pencil-beam scatterometer, measuring radar backscatter at 13.4-GHz in horizontal (HH) and vertical (VV) polarization, at incidence angles of 46° (1400-km swath-width) and 54° (1800-km swath-width), respectively. The 25 × 37 km footprint can be divided by range Doppler filtering into 25 × 6 km slices. Additional filtering, subsampling, and averaging over a 36-h period produces average and standard deviation (STD) images on a 2.225-km grid for both polarizations covering the Arctic and Antarctic on a daily basis [1], [2]. These enhanced resolution products (QS_{er}) are distributed in near-real time by the National Environmental Satellite Data and Information System (NESDIS). Based on these four daily image products, backscatter (σ_{HH} and σ_{VV}) and STD images (STD_{HH} and STD_{VV}) for both polarizations, as well as on the derived active polarization ratio (APR), algorithms to detect four important sea ice parameters, sea ice edge, type, concentration, and drift, have been developed for the Arctic.

These algorithms are run operationally at the Norwegian ice service. Together with ice concentrations (ICs) derived from the Advanced Microwave Scanning Radiometer for Earth Observing System (AMSR-E) and high-resolution synthetic aperture radar (SAR) imagery from Envisat and Radarsat, these QS_{er} sea ice products are today a crucial data set for reliable sea ice monitoring.

In this paper, we will summarize the QS_{er} sea ice algorithms and their results. The sea IC algorithm [3] will be presented more explicitly since the sea ice edge and drift algorithm have already been published in detail in earlier publications [4], [5]. The use of the QS_{er} sea ice products for climate research like the evolution of the global and perennial Arctic ice cover and its export through Fram Strait will be outlined before concluding this paper.

II. Sea Ice Edge

A first version for ice-ocean discrimination from QS_{er} has been developed in [6], but it detected neither low IC, nor thin ice [7]. A refined version to detect also low ICs has therefore been developed to satisfy the requirements of operational ice services [4] and is summarized below.

All measurement variables, i.e., the backscatter in HH (σ_{0H}) and VV (σ_{0V}), the APR and the daily STD of the HH and VV backscatters are strongly correlated with ice types and sensitive to IC [8]. The APR has been defined in [9] as

$$\mathrm{APR} = (\sigma_{0H} - \sigma_{0V})/(\sigma_{0H} + \sigma_{0V}).$$

Manuscript received September 25, 2006; revised February 9, 2007. This work was supported in part by the National Aeronautics and Space Administration under Grant NAG 59366 with the National Ice Center, by the ESA European Space Research Institute under 17060703/I-IW with Met.no, and by the German Research Foundation under DFG-project SFB 512.

J. Haarpaintner is with the Norut IT, 9294 Tromsø, Norway (e-mail: joergh@itek.norut.no).

G. Spreen is with the Institute of Oceanography, University of Hamburg, 20146 Hamburg, Germany (e-mail: gunnar.spreen@zmaw.de).

Digital Object Identifier 10.1109/TGRS.2007.895419

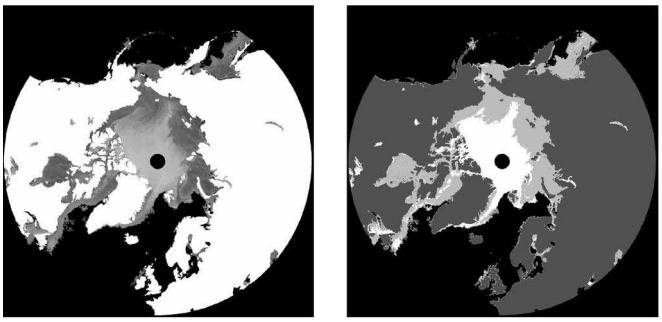

(a) (b)

Fig. 1. Arctic sea ice cover from March 11, 2003: (a) σ_{0H}, and (b) classified into FYI (light gray) and MYI (white).

APR showed to be the crucial variable to separate ice from ocean with a threshold of -0.02. Season-dependent thresholds for the other variables serve to eliminate most of the ocean noise, i.e., ocean pixels falsely classified as ice. The effective QS_{er} resolution is estimated to 5–10 km but the QS_{er} products are subsampled on a 2.225-km grid. Reducing the ice edge resolution to a 6.675-km grid by averaging over a 3×3 pixel window allows us to choose the least ambiguous, i.e., the highest absolute, APR value among the 3×3 pixels. The history of the ice cover is also used to detect individual ice fields that are separated from the Arctic pack and would otherwise be eliminated by filtering. Fig. 1(a) shows an example of the sea ice edge detection over the whole Arctic from March 11, 2003. The validation study showed that ICs as low as 10% can be detected by this algorithm. Strong melting events during summer can cause strong daily variations in the backscatter and increase the daily STD and thus falsely classify ice as open water. However, such errors can be easily eliminated by comparing subsequent days.

III. Sea Ice Type

Multiyear (MYI) and first-year (FYI) ice have different salt contents. Since scatterometer radar pulses have a deeper penetration depth in fresh ice than in ice containing brine pockets, the backscatter of MYI is characterized by stronger volume scattering than FYI and appears therefore brighter in the satellite images with a higher backscatter coefficient. A good threshold for separating MYI from FYI is around -12 dB [4]. Other factors, like flooding, melting, and refreezing of the surface ice layer can change the salt water content in the ice independently of the ice age and change the backscatter. In the Arctic, such events occur mainly in the marginal ice zone (MIZ) or during summer. Snow cover changes (layering, surface roughness and snow grain size) are also responsible for backscatter variability. Fig. 1(b) shows the classified image of Fig. 1(a) into FYI and MYI.

IV. Sea Ice Concentration

QS_{er} products were colocated and statistically analyzed with special sensor microwave/imager (SSM/I) NASA-team (NT) IC maps over the whole Arctic ice cover. The statistical analysis revealed that there is an obvious signature of the total IC in

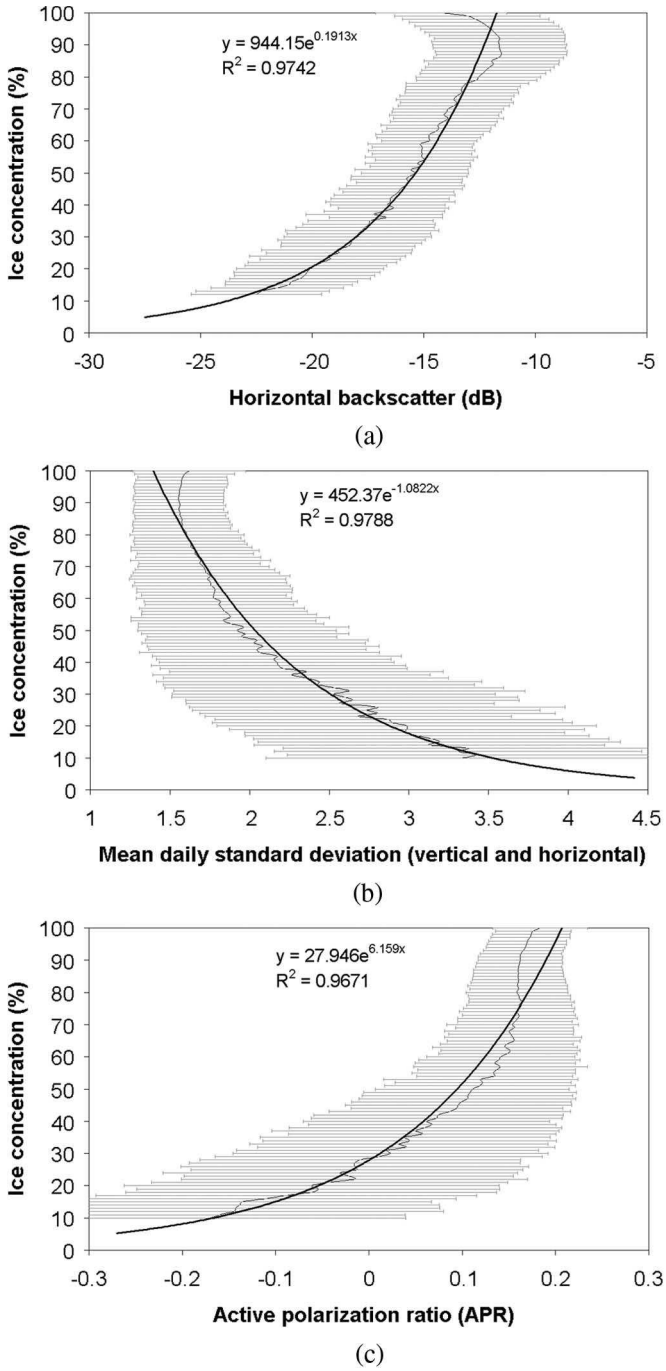

Fig. 2. Colocation of SSM/I NT IC and QS variables: (a) σ_{0H}, (b) STD, and (c) APR. The thin lines are mean values for each IC averaged over the first day of all months and error bars indicate $\pm$ one STD. Thick lines are regression lines with equations.

the available QS parameters: σ_{HH}, σ_{VV}, STD_{HH}, STD_{VV}, and APR (Fig. 2). Exponential regression lines for IC as a function of QS variables revealed correlation coefficients R^2 greater than 0.95 (Fig. 2) with yearly mean values for SSM/I IC. However, STDs are of the order of $\pm 30\%$ IC. It is therefore necessary to combine the different parameters to determine IC. The regression equations of Fig. 2 are used to determine the IC from QS data alone for the whole Arctic at 6.675-km resolution 1) for each individual parameter and 2) for a combination of different parameters and their regression equations.

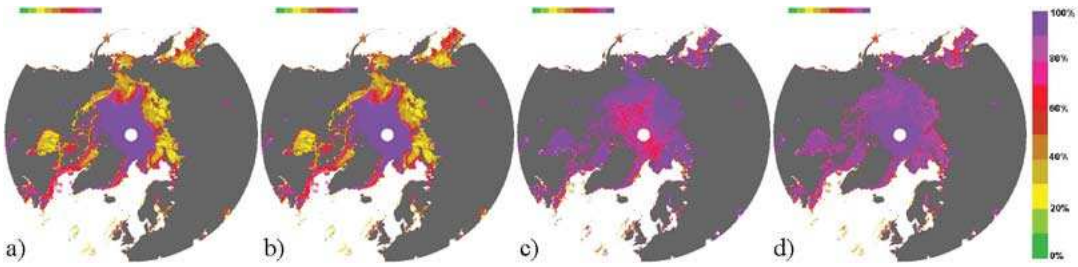

Fig. 3. IC maps from individual parameters (a) $\mathrm{IC_{HH}}$, (b) $\mathrm{IC_{STD}}$, (c) $\mathrm{IC_{APR}}$, and (d) from the combination of all of them on March 11, 2003.

A. Ice Concentration From Individual QS Parameters

The IC from the individual parameters $\sigma_{0\mathrm{H}}$, mean($\mathrm{STD_{HH}}$, $\mathrm{STD_{VV}}$), i.e., $\mathrm{IC_{STD}}$, and APR are described here.

1) IC_{HH}: Fig. 2(a) shows that the backscatter increases with higher ICs. As said earlier the backscatter is mainly driven by the ice type. Low ICs occur however mainly in the MIZ, which in winter is composed dominantly by FYI. Studying the derived IC from $\sigma_{0\mathrm{H}}$ alone shows therefore that it corresponds more to the ice-type composition than to the real IC. In addition, surface roughness has also a strong impact on the backscatter and ridged FYI fields appear therefore also as higher IC. $\sigma_{0\mathrm{H}}$ is therefore unsuitable to determine IC by itself. The dependence of $\sigma_{0\mathrm{V}}$ on IC is similar but about 2 dB smaller because of the higher incidence angle.

2) IC_{STD}: $\mathrm{STD_{HH}}$ and $\mathrm{STD_{VV}}$ are similar and we use therefore their mean value (STD) in this comparison. Fig. 2(b) shows that STD decreases with higher ICs. STD is mainly dominated by the daily backscatter variation over open water due to the highly variable ocean surface, as well as the different azimuth angles of the multiple observations per pixel. Inside the pack ice, STD is slightly lower for MYI than for FYI. One reason could be that dominating volume scattering in MYI is less sensible to different azimuth angles. The backscatter of FYI is also more variable because of stronger thermodynamic and kinetic variability of its surface. The derived IC is therefore slightly higher for MYI than for FYI. Along the MYI/FYI border, STD increases due to dynamics in the ice cover and the strong variation along the MYI/FYI border, and shows therefore lower IC. Along the MIZ, the effect of higher STD over open water seems to give reasonable results in order to reflect the IC.

3) IC_{APR}: Fig. 2(c) shows higher APR values with higher ICs. APR is higher for FYI than for MYI [4]. FYI regions appear therefore as higher IC and APR varies little for IC above 50%. Below 50% however, it seems that the open ocean has a stronger effect in reducing the APR than the different ice types. The APR seems therefore to be a good parameter to determine IC in the MIZ.

B. Combining the Different Parameters to Determine the Ice Concentration

Individual parameters are unreliable alone to determine the IC over the whole Arctic region. However, each of them presented some characteristics for different ice regions that could be used in a combination of all of them to better determine the IC from QS. We therefore divide the Arctic ice cover first into these regions of different ice types: MYI, FYI, and the MIZ. The FYI/MYI areas are separated by $\sigma_{0\mathrm{H}}(\mathrm{FYI}) < -12$ dB $< \sigma_{0\mathrm{H}}(\mathrm{MYI})$ and we define the MIZ as a 20-pixel ($\sim$125 km) large belt along the ice edge. We then propose the following empirical combinations of the ICs from the individual parameters, based on the results above.

$$\mathrm{IC(MYI)} = \max(\mathrm{IC_{APR}}, \mathrm{IC_{STD}}) \tag{1}$$

$$\mathrm{IC(FYI)} = \left(\max(\mathrm{IC_{HH}}, \mathrm{IC_{STD}}) + \mathrm{IC_{APR}}\right)/2 \tag{2}$$

$$\mathrm{IC(MIZ)} = (\mathrm{IC_{HH}} + \mathrm{IC_{STD}} + \mathrm{IC_{APR}})/3 \tag{3}$$

where $\mathrm{IC_{HH}}$, $\mathrm{IC_{STD}}$, $\mathrm{IC_{APR}}$ are the ICs from individual parameters. In the MIZ (3), we use the average of all single-parameter ICs since all parameters showed a reasonable decrease of IC toward the ocean. The purpose of (1) and (2) is to maximize the IC in the pack ice region. Fig. 3 shows the Arctic IC for each individual parameter and for the combination for March 11, 2003. The results are then classified into 10% bins: 1%–10%, 11%–20%, etc.

C. Results and Validation

The IC are averaged over 3×3 pixel to adapt them to the usual 25-km resolution from SSM/I. Fig. 4 shows the IC results in 6.675- and 20-km resolution compared to higher resolution satellite imagery. Although very empirical, the combined IC gives qualitatively reasonable results, separating well into high and low ICs: high IC ($> 80\%$) over the whole Arctic pack ice [Fig. 3(d)] and decreasing IC in the MIZ toward the ice edge. Some individual ice features could even be resolved in the highly dynamic Fram Strait during summer, including polynyas and very low IC in the Greenland Sea [Fig. 4(d)–(f)]. Quantitatively however the ICs are not very accurate since IC in the high Arctic should be above 99%. For a more quantitative validation, the ten IC classes have been collocated with SSM/I NT total ICs. Fig. 5 shows the histogram for each class, showing that ICs above 80% are relatively well defined with STDs below 15%. Classes between 21% and 80% are not accurate and have a widespread probability distribution and STDs above 20%. The two lowest IC classes (1%–20%) show well-defined peaks in their probability distribution for low IC.

We conclude that although not very accurate, the IC algorithm allows at least a separation into three IC classes: low (1%–20%), mean (21%–79%) and high ($> 80\%$) IC. It should be mentioned that the NT algorithm has its problems, too, particularly for high ICs [10], which may account for some of the differences between the two algorithms.

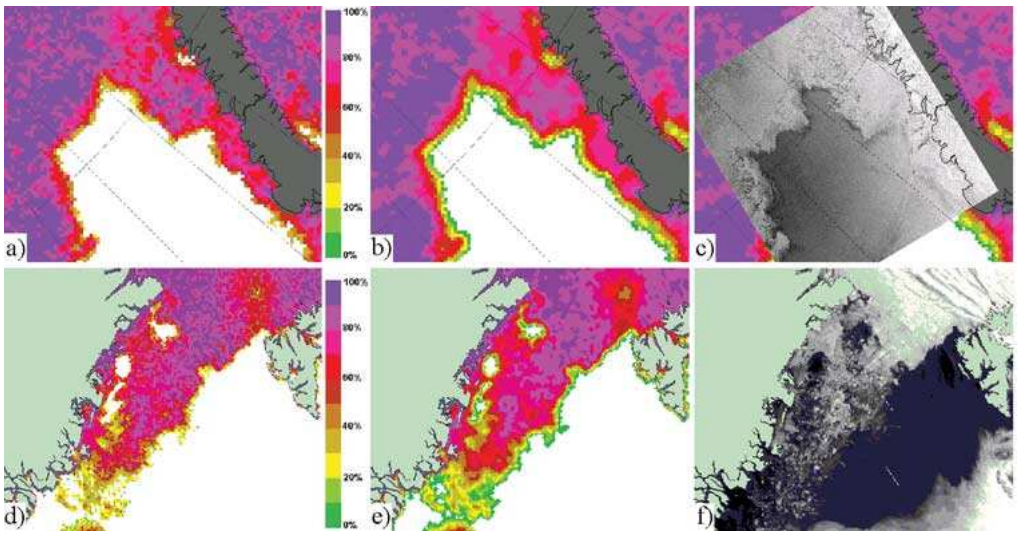

Fig. 4. IC results in (a) 6.675- and (b) 20-km resolution compared to a (c) Radarsat SAR image (Canadian Space Agency) in the eastern Barents Sea in winter (March 11, 2003), and (d) 6.675- and (e) 20-km resolution compared to a (f) AVHRR (NOAA) image (1-km res.) in Fram Strait in summer (July 21, 2003).

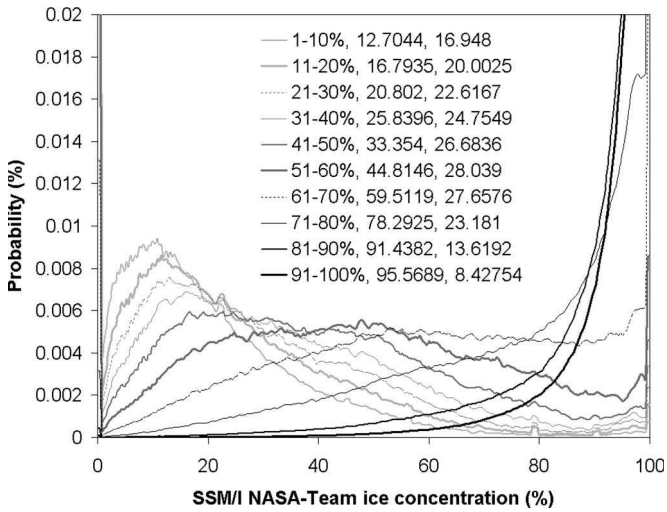

Fig. 5. Histograms of the ten IC classes from collocation with SSM/I NT ICs. The inserted table indicates the QS IC range, the mean IC and STD for each class in SSM/I NT data.

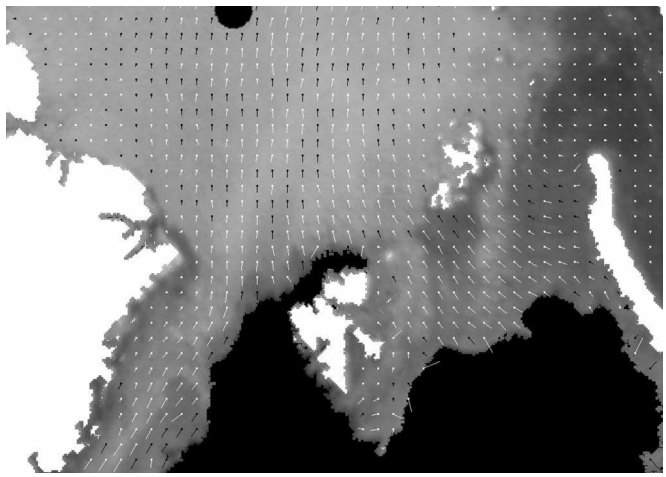

Fig. 6. 48-h QS_{er} ice drift in the European Arctic from March 11, 2003 to March 13, 2003. White drift vectors (flags) are calculated by MCC, black drift vectors are filtered and then interpolated drift vectors.

V. Sea Ice Drift

Sea ice drift can be determined from QS_{er} imagery by maximum cross correlation (MCC), which has been published previously [5]. This section will summarize the method and validation results.

Correlation windows of 61 $\times$ 61 pixel have been used to calculate the MCC for both polarizations independently for images separated by 2 days. Erroneous drift vectors can easily be eliminated by comparing the two resulting 48-h ice drift vectors, $\overrightarrow{u_{\mathrm{VV}}}$ and $\overrightarrow{u_{\mathrm{HH}}}$. Additional filtering is performed by setting a minimum correlation coefficient and by considering the spatial consistency of the motion field. Eliminated vectors are reconstructed by interpolation. The results have been validated with buoy positions from the International Arctic Buoys Program showing an error STD in ice drift speed of 2.6 cm/s for a 48-h drift. Typical ice drifts are in the range of 10–15 cm/s in the Arctic but can easily exceed the double in Fram Strait. Since QS_{er} data is averaged over a 36-h period, we expect that the largest part of the error is due to the smearing effect of ice motion during the integrating period (see [5] for more details). Errors are largest in dynamic regions with low ICs like the southern Greenland Sea. Fig. 6 shows an example of ice drift in the European Arctic with the transpolar drift and the Fram Strait outflow. Ice drift data derived from QS_{er} have been used in connection with ice thickness measurements from ICESat in order to estimate the sea ice volume flux through Fram Strait in 2003 [11] with results comparable to historical mean values [12], [13]. Section VI-B will develop this further.

VI. Enhanced Resolution QS for Climate Research

Rather than presenting a complete climatic analysis for QS' lifetime, this section will outline some ideas of the possible use of QS_{er} for climate research. QS has been reliably in operation since September 1999. A more than 7-year time series of

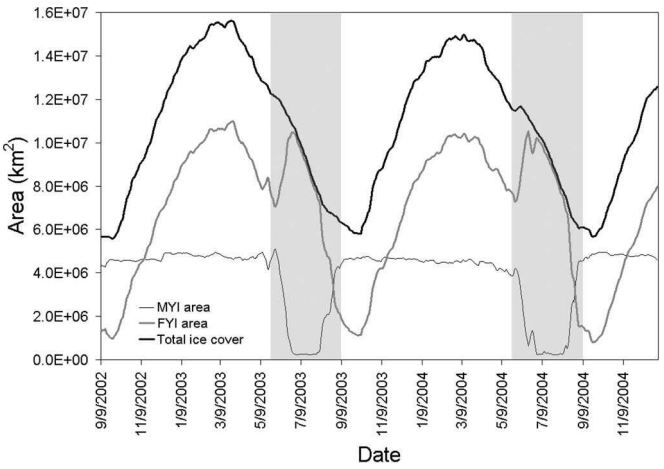

Fig. 7. Seasonal evolution of the total Arctic ice cover, the MYI and the FYI areas from September 2002 to December 2004. Melting periods are marked as gray bars.

daily global observations is therefore available over the whole Arctic region and represents an important climatic data set. The authors have processed QS_{er} data only for the period September 2002 to December 2004.

A. Seasonal Evolution of the Total, MYI, and FYI Arctic Ice Cover

The ice edge algorithm has been shown to be reliable [4]. By applying a seven-day running mean over the processed time series, ocean noise can easily be eliminated. As in III the total ice cover can also be separated into MYI and FYI area. Fig. 7 shows the evolution of the total ice cover, the perennial ice (MYI), as well as the FYI area, assuming 100% ice cover for each ice pixel of either class. During summer, the ice cover cannot be separated into MYI and FYI because of surface melting events. The melting periods area marked as gray bars in Fig. 7.

We estimate the maximum error of the total ice extent to ± 1 pixel along the ice edge, which adds up to $\pm 2.5 \times 10^5$ km^2 for the whole Arctic. We assume this error for all following ice extent quantities. For the winters 2003 and 2004, the maximum Arctic ice extends are 15.6×10^6 and 15.0×10^6 km^2, respectively. The minimum ice extends are 5.81×10^6 (October 8, 2003) and 5.66×10^6 km^2 (September 23, 2004). The minimum ice extend for 2002 of 5.58×10^6 km^2 on September 25 is also shown in Fig. 7. FYI varies in the range 1–11×10^6 km^2 and is responsible for most of the seasonal variation of the total ice cover. The processed time series a little over 2 years is too short to conclude on any climate change aspects, but gives a range of seasonal and interannual variability.

The MYI area is relatively stable during the year. Its maximum extend is defined by the ice cover that has not been melted away during summer and lost most of its brine content by drainage during aging and the melting season. The decrease of MYI from autumn to summer is governed by the ice export mainly through Fram Strait; to a minor extend also through the Barents Sea and the Canadian Archipelago, and by deformation. From October 1, 2003 to June 1, 2004, the MYI area estimated by QS decreased by about 0.66×10^6 km^2 from

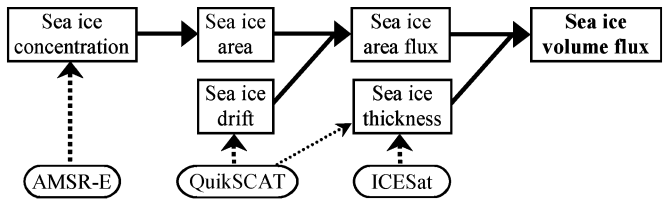

Fig. 8. Schematic flow diagram of quantities (boxes) and satellites/sensors (ovals) involved in the estimation of the sea ice volume flux.

4.67×10^6 to 4.01×10^6 km^2, and is comparable to the average winter ice area flux through Fram Strait of 0.75×10^6 km^2 in [12]. Using QS ice drift for 2003/2004 the winter ice area flux through Fram Strait (see Section VI-B) at 79° N has been calculated to about $(0.46 \pm 0.09) \times 10^6$ km^2, assuming 100% IC per pixel. This area is smaller but of the same order as the MYI area decrease. Taken into account that additional MYI has been exported through the Barents Sea and the Canadian Archipelago, this result compares well with the MYI area decrease.

B. Sea Ice Volume Flux Through Fram Strait

The sea ice export through Fram Strait is the single largest fresh-water source of the Greenland Sea. It is highly variable and amounts annually to about 10% of the total Arctic sea ice mass [14]. The here presented QS_{er} sea ice drift data (Section V) can be used in conjunction with sea ice thickness and area data to estimate the sea ice volume flux (Fig. 8).

Sea ice thickness is derived from ICESat/GLAS [15] laser altimeter measurements. ICESat measures the elevation of the Earth surface above a reference ellipsoid every 170 m in a 64 m diameter laser footprint. In ice covered regions these measurements originate from the sea ice top, including the snow, the open water or thin ice in leads. By assuming the lowest measured elevations to be the sea surface height (SSH) the sea ice freeboard height, including the snow cover can be obtained by subtracting the SSH from the remaining elevation measurements [11]. The feasibility of this approach was shown by comparison with SAR data [16]. The freeboard heights are converted to sea ice thickness by assuming isostatic equilibrium and using fixed values for the snow, water, and ice densities. Snow depth is taken from climatology in combination with *in situ* measurements from 2003. Different ice densities are applied to FYI and MYI, which are discriminated by use of QS data. Sea ice area is calculated with the ARTIST sea IC algorithm using AMSR-E 89-GHz radiometer data [17], [18].

ICESat is not measuring continuously but for three measurement periods of approximately one month per year, hereafter referred to as period February/March 03 (February 20–March 19, 2003), October/November 03 (September 29–November 18, 2003), and February/March 04 (February 18–March 20, 2004). All valid ICESat ice thickness data of each measurement period is averaged on a 25-km polar stereographic grid. The number of measurements per grid cell distribution has a strong south–north gradient depending on ICESat overpasses, increasing from approximately 150 (one overpass) up to 4500 measurements per grid cell near 86° N. At 80° N, the ice thickness is in general the mean of several overpasses. Since ice thickness is a slowly changing parameter compared to the

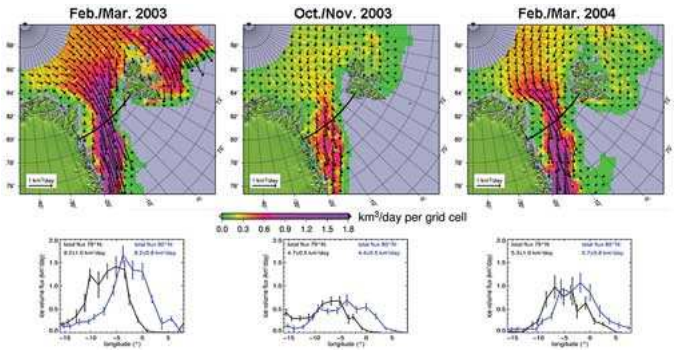

Fig. 9. Mean daily sea ice volume flux in the Fram Strait region for periods (left) February 20 to March 19, 2003, (center) September 29 to November 18, 2003, and (right) February 18 to March 20, 2004. Top panels show the spatial distribution of the volume flux with colors encoding the absolute amount of volume flux out of every grid cell and vectors for every third grid cell display the direction and amount. Gray areas denote either open water or missing data. Bottom panels show the zonal distribution of the meridional volume flux through a transect (black line in top panels) at 79° N (black) and 80° N (blue); error bars denote the RMS error budget of the transect data points.

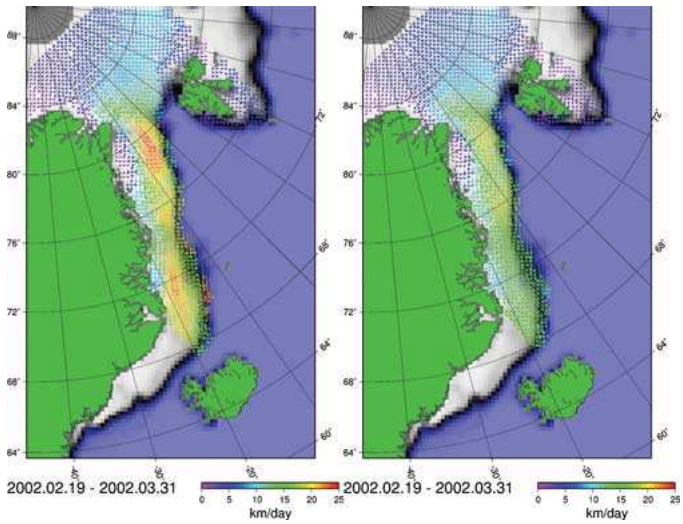

Fig. 10. Mean daily QS_{er} sea ice drift during the period February 19 to March 31, 2002. The left panel was calculated by cross correlation from QS_{er} data with one-day time leg, the right panel with a two-days time leg.

ice drift, monthly averaging can therefore balance poor sampling. Sea ice area from AMSR-E and drift from QS_{er} are calculated or interpolated on the same grid, respectively. In contrast to the study in [11], we are here inter- or extrapolating the ice drift to all ice covered regions with a maximum distance of 100 km to the next data point using a continuous curvature with tension interpolation. Additionally the averaged ice thickness data are interpolated for all regions with available ice drift using kriging interpolation. This is expected to give more accurate results, particularly in the MIZ, where the ice drift data density is quite low and thus single drift estimates were dominating the complete averaging period. Missing grid points in the ice thickness data were causing discontinuities in the meridional ice volume flux along the East Greenland Current (EGC).

Sea ice volume fluxes are calculated according to the scheme in Fig. 8 for the three ICESat measurement periods and are shown in Fig. 9. The top panels show the spatial distribution of the sea ice volume flux. This became possible for the first time with the use of ICESat data. Before, all measured volume fluxes were based on pointwise sea ice thickness measurements obtained from upward looking sonar (ULS) data. The bottom panels present the meridional volume flux across two transects at 79° N (black curves) and 80° N (blue curves). During all three periods fluxes are highest in the center of the EGC. In the western part of Fram Strait, nondrifting land-fast ice prevails attached to the Greenland coast. In the eastern part, low IC is causing small ice volume flux despite the high drift speeds. Clearly, the seasonal cycle between the two winter periods February/March 03 and 04 and the fall period October/November 03 is visible. But also the interannual variation between February/March 03 and February/March 04 becomes clear. While in February/March 03 strong fluxes from the north with an additional inflow of thick ice from the north of Greenland dominate the Fram Strait region, in February/March 04 the fluxes are much smaller and tend to originate more from the transpolar drift and the north–east of Svalbard.

By integrating the meridional fluxes along the 79° N transect the total Fram Strait export out of the Arctic Ocean into the Greenland Sea can be obtained. For a 30-day month, the export accounts for 276 ± 30 km^3/month in February/March 03, 141 ± 15 km^3/month in October/November 03, and 159 ± 30 km^3/month in February/March 04. These results are comparable to results of other studies using ULS data; the mean flux and STD for February/March and October/November during the years 1991 to 1996 were 290 ± 80 km^3/month and 183 ± 101 km^3/month according to [12], and 348 ± 181 km^3/month and 247 ± 110 km^3/month according to [13], respectively. For comparison, we also calculated the sea ice volume flux using the method described above using ice drift derived from AMSR-E 89-GHz data [19] instead of QS_{er}. The sea ice export through the 79° N transect then adds up to 318 ± 36 km^3/month for February/March 03, 204 ± 21 km^3/month for October/November 03, and (303 ± 51) km^3/month for February/March 04. The differences between the two series of flux estimates, using QS_{er} and AMSR-E drifts for the same periods, are due to the different data density distribution of the ice drift datasets in this dynamic region and differences between the two drift datasets. In general, there is less AMSR-E ice drift data available in the Greenland Sea than QS_{er} drift. But high ice drift speeds may not be correctly detected in the EGC with the standard two-day drift of the QS_{er} correlation method. Fig. 10 shows the mean daily ice drift during February 19 to March 31, 2002 for a one-day drift (left panel) and standard two-day drift (right panel). The drift speed is clearly higher in the EGC for the one-day MCC. Although there could be identical data in two successive QS_{er} datasets, as QS_{er} data are integrated over a 36 h period, there are more high-speed ice drift vectors found. After two days, some QS_{er} patterns might be already decorrelated and thus are no longer detected. These issues will be further investigated.

VII. Conclusion

In this paper, we summarized the algorithms to extract four important sea ice parameters (edge, type, concentration, and drift) from QS_{er} data with a more detailed description

of the sea IC algorithm. Ice thickness cannot be determined from QS. These algorithms have been implemented in the daily operations at the Met.no ice service and significantly improved the accuracy of the produced sea ice charts. After seven years of operation, QS presents an important data set for climate research. Two main aspects of how these data products can be used for climate research are shown. The estimation and evolution of the total and perennial ice cover can easily be extracted using the ice edge and ice-type algorithms. By combining the ice drift from QS_{er} with the ICs from AMSR-E and ice thickness measurements from ICESat, the ice volume export through Fram Strait can also be estimated. Due to the high ice drift through Fram Strait, the MCC method applied on a 1-day ice drift instead of a 2-day drift might give more accurate results. It would be necessary to process the complete QS data set and combine it with other global data sets to conclude further on climate change aspects.

Unfortunately, ADEOS-II who carried the follow-up of the SeaWinds sensor failed nine months after its launch in 2003 and the continuity of this data set is at risk. The recently started (October 19, 2006) European series of polar orbiting satellites for operational meteorology (MetOp) carries the Advanced SCATterometer (ASCAT) and will hopefully provide a continuous scatterometer data set until 2019. A future challenge is to adapt the above algorithms to ASCAT who operates in C-band single polarization. It is planned to produce also enhanced-resolution products from ASCAT.

ACKNOWLEDGMENT

The authors would like to thank National Oceanic and Atmospheric Administration (NOAA)/NESDIS for providing the QS_{er} data that have been developed by D. G. Long (Brigham Young University), to NSIDC for providing the ICESat, SSM/I and AMSR-E data, to M. Porcires, R. R. Tonboe, S. Kern, and R. Ezraty for useful discussions, and to the two anonymous reviewers.

REFERENCES

[1] D. G. Long, P. J. Hardin, and P. T. Whiting, "Resolution enhancement of spaceborne scatterometer data," *IEEE Trans. Geosci. Remote Sens.*, vol. 31, no. 3, pp. 700–715, May 1993.

[2] D. S. Early and D. G. Long, "Image reconstruction and enhanced resolution imaging from irregular samples," *IEEE Trans. Geosci. Remote Sens.*, vol. 39, no. 2, pp. 291–302, Feb. 2001.

[3] J. Haarpaintner and M. Porcires, "On the sea ice concentration from enhanced resolution QuikScat/Seawinds data," presented at the Eur. Geosciences, 1st General Assembly Union, Nice, France, Apr. 25–30, 2004.

[4] J. Haarpaintner, R. T. Tonboe, D. G. Long, and M. L. VanWoert, "Automatic detection and validity of the sea ice edge: An application of enhanced resolution QuikScat/SeaWinds data," *IEEE Trans. Geosci. Remote Sens.*, vol. 42, no. 7, pp. 1433–1443, Jul. 2004.

[5] J. Haarpaintner, "Arctic-wide operational sea ice drift from enhanced resolution QuikScat/seaWinds scatterometry and its validation," *IEEE Trans. Geosci. Remote Sens.*, vol. 44, no. 1, pp. 102–107, Jan. 2006.

[6] Q. P. Remund and D. G. Long, "Sea ice extent mapping using Ku-band scatterometer data," *J. Geophys. Res.*, vol. 104, no. C5, pp. 11 515–11 527, 1999.

[7] R. De Abreu, K. Wilson, M. Arkett, and D. Langlois, "Evaluating the use of QuikSCAT data for operational sea ice monitoring," in *Proc. IEEE Int. Geosci. and Remote Sens. Symp.*, Toronto, ON, Canada, Jun. 2002, pp. 3032–3033.

[8] R. Tonboe and J. Haarpaintner, "Implementation of QuikScat/SeaWinds data in the EUMETSAT ocean & sea ice ice product," Danish Meteorological Inst., Copenhagen, Denmark, Tech. Rep. 03-13, 2003, 41 pp.

[9] R. Tonboe and R. Ezraty, "Monitoring of new-ice in Greenland waters," in *Proc. IEEE Int. Geosci. and Remote Sens. Symp.*, Toronto, ON, Canada, Jun. 2002, pp. 1932–1934.

[10] J. C. Comiso, D. J. Cavalieri, C. L. Parkinson, and P. Gloersen, "Passive microwave algorithms for sea ice concentration: A comparison of two techniques," *Remote Sens. Environ.*, vol. 60, no. 3, pp. 357–384, 1997.

[11] G. Spreen, S. Kern, D. Stammer, R. Forsberg, and J. Haarpaintner, "Satellite-based estimates of sea ice volume flux through Fram Strait," *Ann. Glaciol.*, vol. 44, 2006. in press.

[12] R. Kwok, G. F. Cunningham, and S. S. Pang, "Fram Strait sea ice outflow," *J. Geophys. Res.*, vol. 109, no. C1, p. C01009, 2004.

[13] T. Vinje, N. Nordlund, and A. Kvambekk, "Monitoring ice thickness in Fram Strait," *J. Geophys. Res.*, vol. 103, no. C5, pp. 10 437–10 449, 1998.

[14] K. Aagaard and E. Carmack, "The role of sea ice and other fresh water in the Arctic circulation," *J. Geophys. Res.*, vol. 94, no. C10, pp. 14 485–14 498, 1989.

[15] H. J. Zwally, B. Schutz, W. Abdalati, J. Abshire, C. Bentley, A. Brenner, J. Bufton, J. Dezio, D. Hancock, D. Harding, T. Herring, B. Minster, K. Quinn, S. Palm, J. Spinhirne, and R. Thomas, "ICESat's laser measurements of polar ice, atmosphere, ocean, and land," *J. Geodyn.*, vol. 24, no. 3/4, pp. 405–445, 2002.

[16] R. Kwok, H. J. Zwally, and D. Yi, "ICESat observations of Arctic sea ice: A first look," *Geophys. Res. Lett.*, vol. 31, no. 16, p. L16401, 2004.

[17] L. Kaleschke, C. Lüpkes, T. Vihma, J. Haarpaintner, A. Bochert, J. Hartmann, and G. Heygster, "SSM/I sea ice remote sensing for mesoscale ocean-atmosphere interaction analysis," *Can. J. Remote Sens.*, vol. 27, no. 5, pp. 526–537, 2001.

[18] G. Spreen, L. Kaleschke, and G. Heygster, "Operational sea ice remote sensing with AMSR-E 89 GHz channels," in *Proc. IEEE Geosci. and Remote Sens. Symp.*, 2005, vol. 6, pp. 4033–4036.

[19] R. Ezraty, F. Ardhuin, and D. Croizé-Fillon, "Sea ice drift in the Central Arctic using the 89 GHz brightness temperatures of the advanced microwave scanning radiometer (AMSR-E)," in *User's Manual*. Brest, France: Institut Français de Recherche Pour L'Exploitation de la Mer (IFREMER), 2005. ver. 2.0.

Jörg Haarpaintner received the degree in applied physics and received the Ph.D. degree in physical methods for remote sensing from the University of Versailles-St.Quentin, France, in 2001.

In 2001, he was an EU Fellow, doing research, at the Norwegian Polar Institute in Tromsø, and spending one year at the University Courses on Svalbard. Thereafter, he worked at the Cooperative Research Centre (CRC) for Greenhouse Accounting in Canberra, Australia, before receiving a NASA/UCAR Postdoc grant to join the National Ice Center in Washington, DC. He continued his project at the Norwegian Meteorological Institute in Tromsø, Norway. At Norut IT, since 2005, he has been working on active microwave remote sensing of sea ice, as well as snow, and is responsible for coordinating projects for international sustainable development.

Gunnar Spreen received the M.Sc. degree in physics from the University of Hamburg (UH), Hamburg, Germany, in 2004, where he is currently working toward the Ph.D. at the Institute of Oceanography.

He started to work on sea ice remote sensing at the Institute of Environmental Physics, University of Bremen, Germany, until 2004. Thereafter, he joined the research project "Cyclones and the North Atlantic Climate System" at UH, where he is currently working on a satellite multisensor study to estimate the sea ice freshwater flux. His research interests include active and passive microwave remote sensing, laser altimetry, data analysis, and image processing for polar climate research.